Statistical Mixture Design and Multivariate Analysis of Inkjet Printed a-WO3/TiO2/WOX Electrochromic Films

ARTICLE · DECEMBER 2013

DOI: 10.1021/co400011q · Source: PubMed

4 AUTHORS:

Pawel Jerzy Wojcik

Linköping University, SE-601 74 Norrköping, S…

19 PUBLICATIONS **80** CITATIONS

SEE PROFILE

Luis Pereira

New University of Lisbon

174 PUBLICATIONS **4,078** CITATIONS

SEE PROFILE

R. Martins

Institute for the Development of New Technol…

616 PUBLICATIONS **8,908** CITATIONS

SEE PROFILE

Elvira Fortunato

New University of Lisbon

610 PUBLICATIONS **9,558** CITATIONS

SEE PROFILE

ACS Combinatorial Science

Research Article

pubs.acs.org/acscombsci

Statistical Mixture Design and Multivariate Analysis of Inkjet Printed *a*-$WO_3/TiO_2/WO_X$ Electrochromic Films

Pawel Jerzy Wojcik,* Luís Pereira, Rodrigo Martins, and Elvira Fortunato*

Departamento de Ciência dos Materiais, CENIMAT/I3N, Faculdade de Ciências e Tecnologia, Universidade Nova de Lisboa and CEMOP/Uninova, 2829-516 Caparica, Portugal

Supporting Information

ABSTRACT: An efficient mathematical strategy in the field of solution processed electrochromic (EC) films is outlined as a combination of an experimental work, modeling, and information extraction from massive computational data via statistical software. Design of Experiment (DOE) was used for statistical multivariate analysis and prediction of mixtures through a multiple regression model, as well as the optimization of a five-component sol−gel precursor subjected to complex constraints. This approach significantly reduces the number of experiments to be realized, from 162 in the full factorial ($L = 3$) and 72 in the extreme vertices ($D = 2$) approach down to only 30 runs, while still maintaining a high accuracy of the analysis. By carrying out a finite number of experiments, the empirical modeling in this study shows reasonably good prediction ability in terms of the overall EC performance. An optimized ink formulation was employed in a prototype of a passive EC matrix fabricated in order to test and trial this optically active material system together with a solid-state electrolyte for the prospective application in EC displays. Coupling of DOE with chromogenic material formulation shows the potential to maximize the capabilities of these systems and ensures increased productivity in many potential solution-processed electrochemical applications.

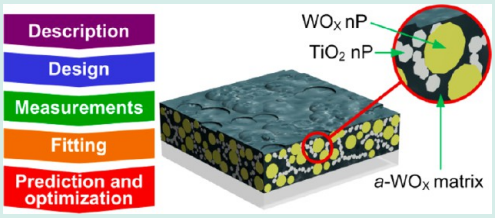

KEYWORDS: *electrochemistry, thin films, mathematical modeling, inkjet printing, tungsten oxide, DOE*

INTRODUCTION

Statistical design of mixture experiments is an established and proven methodology in organic chemistry,[1] biochemistry,[2] environmental science,[3] chromatography,[4] and drug delivery;[5,6] however, so far very few studies have been carried out regarding optimization of solution-processed inorganic EC materials.[7] In this work, thin films are processed by the Inkjet Printing Technique (IPT) which, as an essence of the presented processing method, offers flexibility in deposited film composition, high throughput, and simplicity in material selection, when compared to the conventional methods.[8,9] However, optimization of the printing process by evaluating all possible combinations of factors using single factor experiments is time prohibitive. As there are several factors to evaluate and potential interactions exist between the factors, multifactorial design of experiment (DOE) should be explored as an alternative to traditional single variable experiments. This technique is a time and cost-effective approach for testing the effects of many variables simultaneously. There were three experimental design objectives. To start with, the few important main effects (components) should be selected from the many less important ones. It is also needed to estimate interactions between mixture components and therefore to obtain an idea of the local shape of the response surface one will investigate (development of empirical model). And finally, one has to find the optimum ink composition yielding the most preferable performance of printed EC devices.

The chemical deposition in which a fluid precursor undergoes a chemical change at a solid surface, leaving a solid thin-film, involves formulation (mixture) problems. The discussion presented in this paper concerns the mixture situation in which the proportions of some or all of the components are restricted by constraints, so the entire simplex known from the standard DOE approach cannot be used, and the feasible region is a polytope. In a mixture experiment in general, the independent factors (X_i) are proportions of different components of a blend which must be non-negative and additionally satisfy the condition described by eq 1.

$$\sum_{i=1}^{q} X_i = 1 \tag{1}$$

The response is assumed to depend only on the relative proportions of components present in the mixture and not on the amount of the mixture. Moreover, it is assumed that the errors are independent and identically distributed with a zero mean and common variances.

A common experimental methodology is a full factorial design with all possible combinations of all the input factors. In the case of the constrained mixture design with a specified number of components (q), a full factorial experiment can be

Received: January 16, 2013
Revised: November 19, 2013
Published: December 3, 2013

performed in the proportions or amounts of only $q - 1$ of the components, while the qth stays unused.[10] The qth component can of course be calculated as the missing part of the complete mixture. In a complete experiment, all combinations of the levels (L) of all $q - 1$ factors are tested. The number of experimental runs in the full factorial design grows exponentially with the number of mixture components according to the $L^{(q-1)}$ formula, as it is shown in Figure 1a. Despite the high

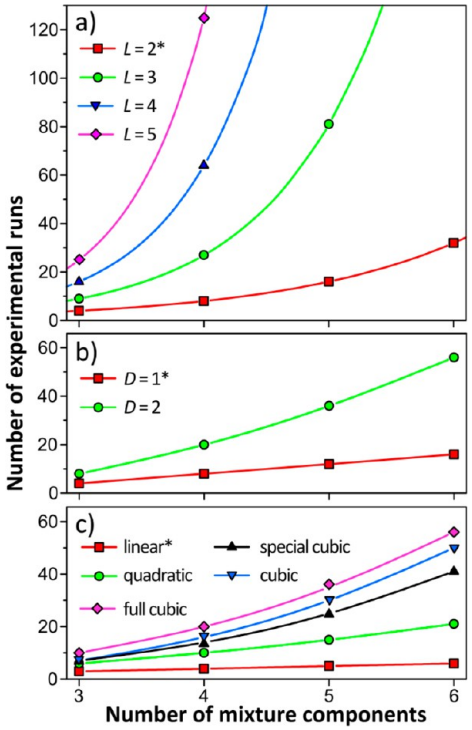

Figure 1. Relationship between minimum number of experimental runs and number of components in the constrained mixture for (a) full factorial (L stands for number of levels), (b) extreme vertices (D stands for a specified degree of midpoints identification), and (c) D-optimal designs. (∗) Number of experimental runs taking under account only main effects.

number of experimental runs, the interpretation of significant terms can be unclear, because variances and covariances of the coefficients can be large. Therefore, the independent variable experiments such as full factorial design are rarely used for blends, and more adequate mixture designs are preferred.

As the mixture experiment with a constrained region is not feasible in the standard mixture design, other designs that cover only a subportion or smaller space within the simplex are required. One approach is called the extreme vertex design,[11] in which all of the vertices of the polytope are used, as well as the centroids of the region, edges, faces, etc. As shown in Figure 1b, the extreme vertex design requires a much smaller number of experimental runs. Another feature is that the region of interest in such a design is defined for mixtures in a more natural way than when using the full factorial approach.

Another approach is to use a D-optimal design provided by a computer algorithm.[12−14] Unlike the standard full factorial design, the computer-aided D-optimal mixture design is always nonorthogonal because effect estimates are correlated. A D-optimal algorithm looks for a design in which the factor effects are maximally independent of each other. This optimality criterion minimizes the generalized variance of the parameter estimates for a prespecified model. Among all known mathematical models considered for mixture experiments in which response surface is continuous over the region being studied, the most usual are Scheffé models[15] expressed by their canonical forms in eqs 2 (linear), 3 (quadratic), 4 (special cubic), 5 (cubic with no main effects), and 6 (full cubic).

$$Y_k = \sum_{i=1}^{q} \beta_i X_i \tag{2}$$

$$Y_k = \sum_{i=1}^{q} \beta_i X_i + \sum_{i=1}^{q-1} \sum_{j=i+1}^{q} \beta_{ij} X_i X_j \tag{3}$$

$$Y_k = \sum_{i=1}^{q} \beta_i X_i + \sum_{i=1}^{q-1} \sum_{j=i+1}^{q} \beta_{ij} X_i X_j + \sum_{i=1}^{q-2} \sum_{j=i+1}^{q-1} \sum_{k=j+1}^{q} \beta_{ijk} X_i X_j X_k \tag{4}$$

$$Y_k = \sum_{i=1}^{q-1} \sum_{j=i+1}^{q} \beta_{ij} X_i X_j + \sum_{i=1}^{q-2} \sum_{j=i+1}^{q-1} \sum_{k=j+1}^{q} \delta_{ij} X_i X_j (X_i - X_j) + \sum_{i=1}^{q-2} \sum_{j=i+1}^{q-1} \sum_{k=j+1}^{q} \beta_{ijk} X_i X_j X_k \tag{5}$$

$$Y_k = \sum_{i=1}^{q} \beta_i X_i + \sum_{i=1}^{q-1} \sum_{j=i+1}^{q} \beta_{ij} X_i X_j + \sum_{i=1}^{q-2} \sum_{j=i+1}^{q-1} \sum_{k=j+1}^{q} \delta_{ij} X_i X_j (X_i - X_j) + \sum_{i=1}^{q-2} \sum_{j=i+1}^{q-1} \sum_{k=j+1}^{q} \beta_{ijk} X_i X_j X_k \tag{6}$$

The function expressed by eq 2 connects each characteristic response (Y_k) with defined q factors (X_i) accounting only for main effects (β_i) while the quadratic and cubic functions (eqs 3−6) consider also second (β_{ij}) and third (β_{ijk}) order interactions, respectively. The $X_iX_j(X_i - X_j)$ and $X_iX_jX_k$ terms in eqs 4−6 model cubic blending of binaries and ternaries, respectively. The coefficients of binaries are symbolized by δ_{ij}. All these models differ from full polynomial models, because they do not contain an intercept value (β_o for $i = 0$). Such simplification occurs according to the eq 1. Note that models expressed by eq 2 do not imply an underlying physical relationship connecting responses with independent factors. Rather, this empirical model is used to estimate statistical significance. Just as the quadratic model is an augmented linear model, the cubic ones are augmented quadratic models. The first order quadratic model ($m = 1$) expressed by eq 3 has the ability to supply high regression coefficients while simultaneously minimizing the overall number of coefficients (p) relative to cubic (eqs 4−6) or second order ($m = 2$) models, which can be summarized (excluding the special cubic model) by eq 7.

$$p = \frac{(q + m - 1)!}{m!(q - 1)!} \tag{7}$$

The D-optimal design not only reduces the number of experimental runs as shown in Figure 1c but also keeps the

dx.doi.org/10.1021/co400011q | ACS Comb. Sci. 2014, 16, 5−16

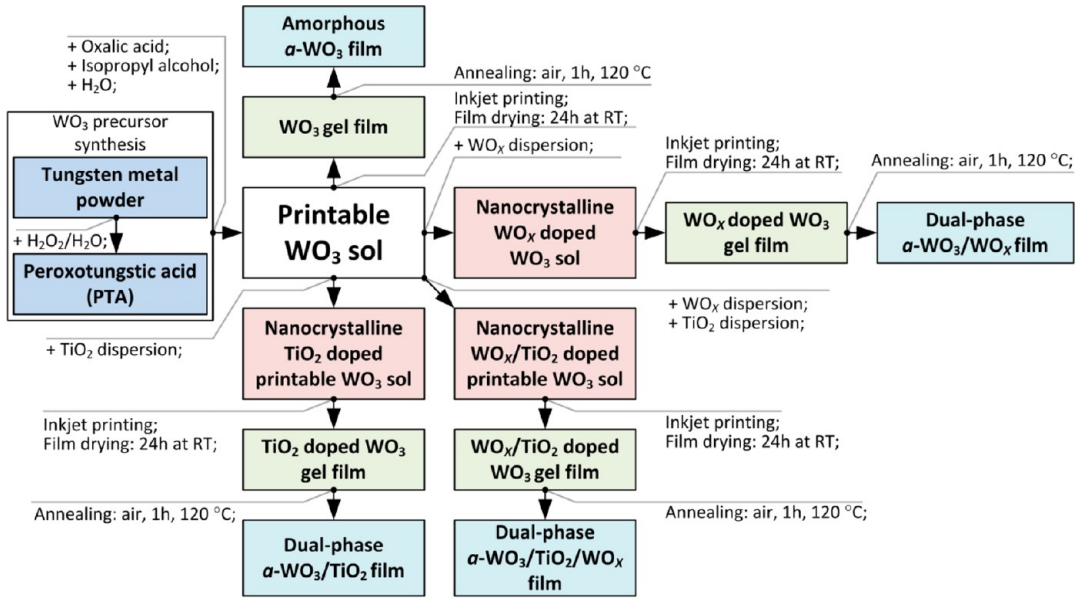

Figure 2. Schematic diagram representing the elements of the studied material system and corresponding technological steps.

more reasonable analysis for the experimental data than the fractional factorial experimental design or extreme vertex design. Additionally, the D-optimal design enables the inclusion of a certain number of experiments already performed and considers them during the analysis, which is not possible in the case of any classical design. D-optimal design seems to be the most powerful tool to cope with a situation when the region of interest is subjected to complex constraints, as the main objective is to conduct reliable analysis of the mixture with the least number of runs. According to this method, a mathematical model is obtained which helps to transport the complexity of studied problem into an easy to handle and practical form.

In the present study, a screening design method has been selected to characterize the inkjet printing process of dual phase a-WO_3/TiO_2/WO_X films, because the problem studied involves a large number of input factors. Such an experimental plan is intended to find the few significant factors from a list of many potential ones and to identify significant effects. The second goal is to build a predictive model for optimization of the ink formulation, which requires precise mathematical modeling. Thus, the DOE approach for mixtures with constraints consists of the following phases: (i) identification of factors (mixture components) that affect the outcome of the experiment and of responses that yield a measure of the outcome, (ii) selection of the appropriate experimental design for screening/surface modeling, (iii) generation of the design matrix, determining which experiments will be conducted, (iv) conducting the experiments and data collection, (v) data fitting and generation of mathematical models for each response, (vi) analysis of significance, (vii) mixture optimization, and (viii) drawing of conclusions.

RESULTS AND DISCUSSION

Design of Experiment. The studied material system shown schematically in Figure 2 can be described as a-WO_3/TiO_2/WO_X, where a-WO_3 stands for an amorphous matrix formed by sol−gel reaction from the PTA precursor, while TiO_2 and WO_X are titanium dioxide and tungsten oxide nanocrystals, respectively. Therefore, films developed based on such a material system can be either amorphous or dual-phase containing one or both kinds of metal oxide. Therefore, the designed mixtures can be described as quinary systems solvent-PTA-OAD-TiO_2-WO_X with one additional nonmixture factor X, which stands for the WO_X nominal particle oxygen content (dual-level categorical factor with values of 2.9 for blue and 3 for yellow nanopowder). Mixtures (inks) must meet strict physicochemical properties (viscosity, surface tension, and maximum particle size) which impose several constraints. The ink composition, based on a solvent with an isopropyl alcohol to water ratio of 0.3:0.7 by weight containing less than 20 wt % of PTA and less than 5 wt % of OAD results in viscosity and surface tension values of 1.5−2 cP and 30−40 dyn cm^{-1}, respectively, acceptable for conventional office printers (see section 2 in the Supporting Information for more details concerning ink rheology adjustment). The maximum nanoparticle size should be at least 100 times smaller than the nozzle diameter (9 μm), i.e., 90 nm (according to Canon FINE technology specification). Additionally, all samples must contain the PTA component (≥1 wt %) in order to ensure the existence of an amorphous phase which guarantees the EC effect by allowing electronic conduction to take place through a low temperature process. On the basis of imposed restrictions, the values of individual weight fraction ranges and categorical levels of factors were defined as follows: $0 \le w_{solvent} \le 0.99$, $0.01 \le w_{PTA} \le 0.2$, $0 \le w_{OAD} \le 0.05$, $0 \le w_{TiO_2} \le 0.99$, $0 \le w_{WO_X} \le 0.99$, $X = \{2.9, \text{blue}; 3:, \text{yellow}\}$. Because of the complexity of such a constricted experimental area, the application of a D-optimal algorithm for experimental design seems essential. A detailed technical description of how a D-optimal design is constructed is beyond the scope of this paper. In simple terms, a D-optimal design is a straight optimization based on both the optimality criterion and the model that will be fitted. The optimality criterion results in minimizing the variance of the parameter estimates for a prespecified model. Based on pre-existing information gained in preliminary experiments, one can hypothesize a more complex model than linear for a mixture under study. Figure 3 shows Average Variance of Prediction calculated by the D-optimal algorithm, as a function of the number of experimental runs. A design that has lower Average

dx.doi.org/10.1021/co400011q | ACS Comb. Sci. 2014, 16, 5−16

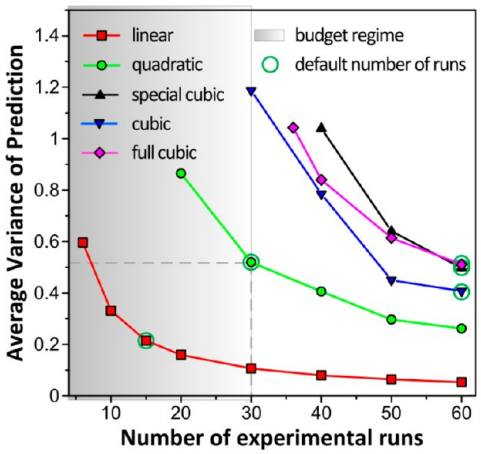

Figure 3. Design diagnostic by evaluation of average variance of prediction as a function of the number of experimental runs for a quinary system with one additional nonmixture factor *X*. The default number of runs suggested by the D-optimal algorithm for each Scheffé model is marked, as well as the determined budged of time and materials.

Variance of Prediction for a considered number of runs is preferred. Therefore, a properly designed experiment originates a low average variance of prediction, while keeping the number of runs within a given budget for the time and materials needed. Supporting a quadratic model requires fewer experimental runs than supporting any of the cubic models and yields a more accurate prediction. Furthermore, the quadratic model is sufficient not only for the screening procedure which enables identification of components of the model that have no effect on the response but also to create the response surface model necessary for the optimization purposes. Briefly, the quadratic, first order polynomial function (Scheffé model) expressed by eq 3 was proposed as an appropriate model for modeling the response data as functions of the so defined mixture components with one categorical factor (see section 7 in the Supporting Information for more details). The minimum number of runs in the computer aided D-optimal design for six factors studied that could fit main effects and two-factor interactions is 20, while the default number suggested by the design generator is 30. As a number of 30 runs does not exceed the available budget for both time and materials, the final design was composed of 30 experiments. Once a decision was made about the mathematical form to fit the responses, the next step was to develop a suitable design of experiments to adequately support such a model. A graphical representation of the generated design is presented in Figure 4 as a ternary plot

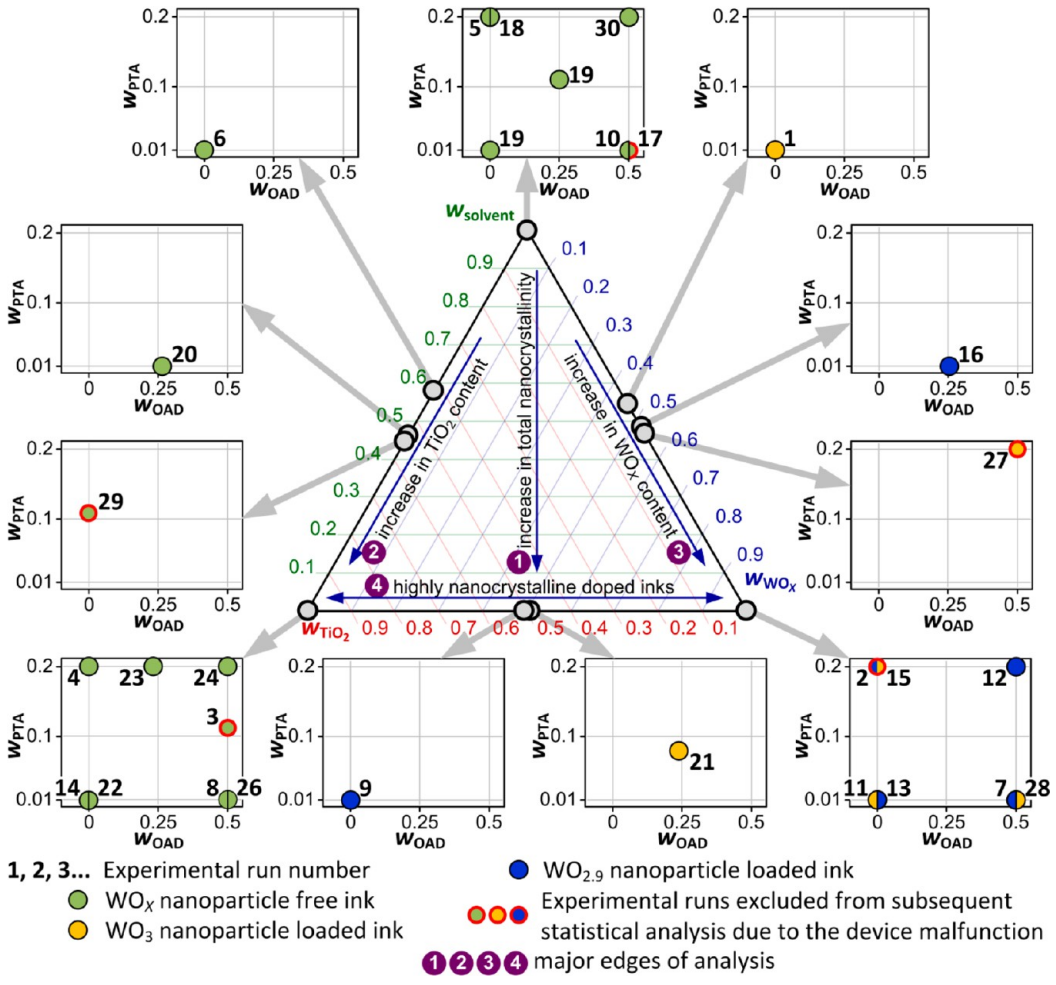

Figure 4. Graphical visualization of the experimental design generated according to the *mixture design with one nonmixture component* methodology for a quadratic Scheffé model. Variables: $w_{solvent}$, w_{PTA}, w_{OAD}, w_{TiO_2}, w_{WO_X}, and *X* stand for weight fractions of solvent, PTA (precursor), oxalic acid, TiO_2 dispersion, WO_X dispersion, and oxygen stoichiometry of WO_X nanocrystals, respectively.

dx.doi.org/10.1021/co400011q | ACS Comb. Sci. 2014, 16, 5−16

($w_{solvent}$, w_{TiO_2}, w_{WO_X}) with 2D subplots (w_{PTA}, w_{OAD}) and colored points (X), enabling the visualization of how all design points were allocated in the design space. It can be observed that the D-optimal design tends to assign design points at the borders and corners of the design space, which is typical for this algorithm. The major edges of analysis were indicated and numbered in the plot according to (1) the increase in nanocrystalline solid concentration at a fixed 1:1 ratio for TiO_2 and WO_X, (2) the increase in concentration of TiO_2 nanocrystals (no WO_X content), (3) the increase in concentration of WO_X nanocrystals (no TiO_2 content), and (4) the proportions of TiO_2 and WO_X dispersions in the ink without pure solvent. The order of runs was fully randomized to minimize the effect of uncontrolled factors that could affect the final result. This is a particular case of the mixture design coupled with one categorical factor which requires the use of a number of runs at least equal to double the number of unknown coefficients in eq 3. Since w_{WO_X} and X factors are dependent, each pair of runs (5, 18), (8, 26), (10, 17), and (14, 22) describes the same experiment. Those experiments cannot be merged, because deleting the duplicates would cause a necessity of a new D-optimal model generation. Ultimately, there were 26 independent runs in D-optimal design and four additional runs serving as checkpoints for the mathematical model. The selected experimental design is sufficient not only to fit the proposed quadratic first order polynomial model but allows testing the model's adequacy as well.

The use of the computer aided D-optimal design successfully reduced the number of overall experimental trials from 162 defined for three-level full factorial design or 72 defined for second-degree extreme vertices design down to 30 runs in the present studies. For each of the experimental runs, a printable solution and targets were freshly prepared just before use in the laboratory experiment.

Fitting of Experimental Data. The design of experiment and statistical data analysis were performed using JMP 8.0 (S.A.S. Institute Inc., Cary, NC, USA). Ternary contour graphical presentations of the models were generated in JMP 8.0 and processed graphically wituy the Visio 2010 (Microsoft Corp., Redmond, WA) diagramming tool.

The mathematical fittings based on multiple regression have been performed for each categorical factor level using the first order polynomial function (quadratic) expressed by eq 8.

$$Y_{1\le k\le 16} = \sum_{i=1}^{5} \beta_i X_i + \sum_{i=1}^{4} \sum_{j=i+1}^{5} \beta_{ij} X_i X_j + \varepsilon \quad (8)$$

Surface responses Y_k ($1 \le k \le 16$) were determined by five controlled mixture components X_i ($1 \le i \le 5$), the coefficients of the main factors, and the coefficients of the first order interactions β_i and β_{ij}, respectively, and ε which represents a random error of the method. This model can be used to predict the response for any condition within the experimental space.

From the measurements of developed devices, 16 responses were obtained: mechanical, optical, electrical, fluidic (ink), and overall performance parameters. Because of the complexity of analysis and the high number of studied responses, the considerations are limited to the main parameters that describe switching kinetics and overall performance of EC films, namely coloration time (τ_{col}), bleaching time (τ_{bl}), optical density (ΔOD), and coloration efficiency (CE; see section 6 in the Supporting Information for definitions). The measured values of selected parameters corresponding to each experimental run are presented in Table 1.

Table 1. Measured Values of Selected Parameters Corresponding to Each Experimental Run

run[a]	τ_{col} (s)	τ_{bl} (s)	ΔOD ($\times 10^{-2}$)	CE ($cm^2\ C^{-1}$)
1	14	9	36.18	188.42
(2)				
(3)				
4	2[b]	3	4.25	29.13
5	3	4	11.5	83.95
6	4	5	46.05	225.72
7	9	4	8.25	70.51
8	4	4	3.84	34.87
9	10	7	37.73	474.01[c]
10	4	3	10.23	73.6
11	4	2[b]	23.31	187.99
12	11	9	38.72	175.2
13	10	7	26.85	80.88
14	3	3	50.98	383.31
(15)				
16	8	6	4.5	15.29
(17)				
18	6	2[b]	1.36[b]	2.84[b]
19	4	8	75.3	404.82
20	2[b]	4	6.95	43.72
21	14[c]	12[c]	82.64[c]	454.09
22	4	5	46.44	305.56
23	4	2[b]	20.72	199.22
24	5	5	18.21	130.05
25	3	2[b]	17.56	91.96
26	8	5	9.39	46.48
(27)				
28	9	2[b]	13.12	48.04
(29)				
30	5	6	55.93	321.43

[a](·) Experimental runs excluded from subsequent statistical analysis due to the device malfunction caused by uncontrollable factors (incorrect encapsulation, film failure, etc.). [b]Minimum response obtained (Y_k^{min}). [c]Maximum response obtained (Y_k^{max}).

A discussion on the microstructural and morphological aspects related to inkjet printed dual-phase a-WO_3/TiO_2/WO_X films is beyond the scope of this paper and is presented elswere.[16] Briefly, the modeled responses presented in Figure 5 were generated at the major edges of analysis defined in Figure 4. By analyzing those plots, it is clear that a substantial reduction in τ_{col} and τ_{bl} values is obtained when increasing the TiO_2 content, while increasing the WO_X content results in the opposite effect. This observation can be explained by increased volume of grain boundaries in highly WO_X doped films, which enhances the trapping of free charge carriers. On the other hand, when increasing the TiO_2 content in the film, the amount of residual charges in a-WO_3/WO_X film decreases due to the enhancement of the reversibility of the redox process. The modeled ΔOD response in Figure 5d indicates that films containing a large amount of TiO_2 nanoparticles (0.76 wt %) with a small share of WO_X content (0.22 wt %) in the amorphous matrix exhibit the highest transmission modulation (ΔOD = 0.38), which is attributed to two mechanisms. First, it is much easier for the TiO_2 nanocrystals to conduct Li^+ ions into the film than for a-WO_3 or WO_X. Second, the TiO_2

dx.doi.org/10.1021/co400011q | ACS Comb. Sci. 2014, 16, 5−16

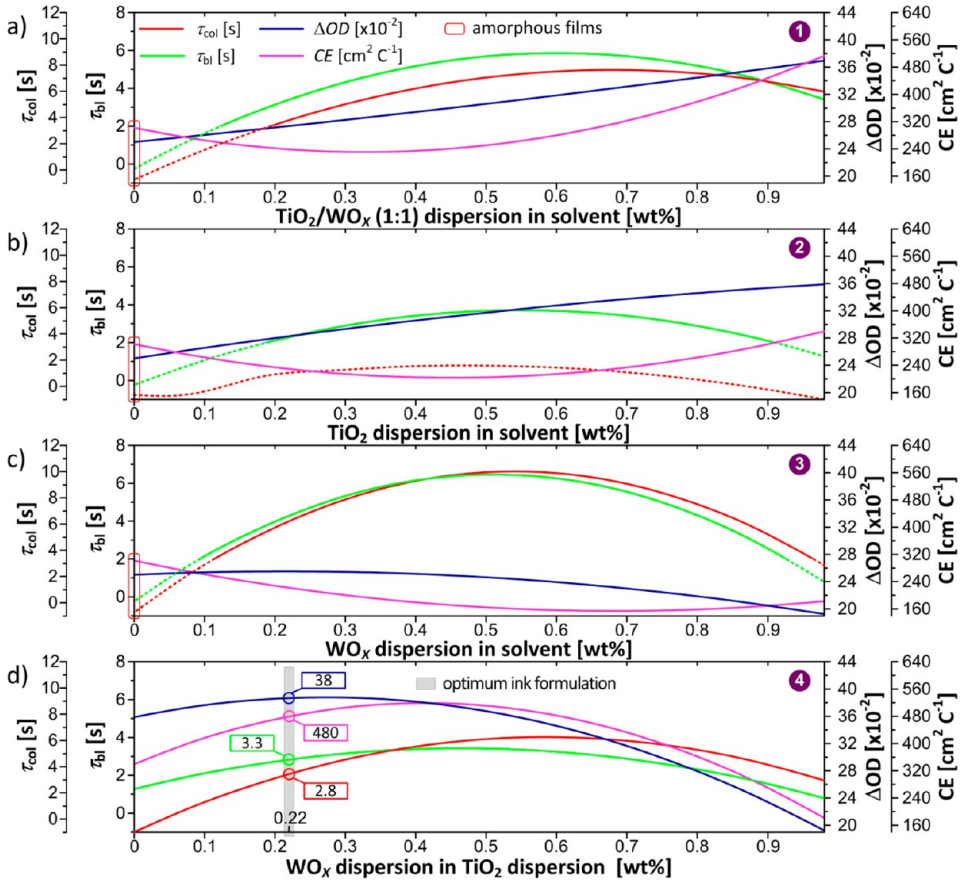

Figure 5. Modeled response plots presenting variation in τ_{col}, τ_{bl}, ΔOD, and CE at the major edges of analysis defined in Figure 4. w_{PTA} = 0.01, w_{OAD} = 0.01, X = 3{yellow}; dashed line represents physically unreliable data (values of τ_{col} and τ_{bl} below 2 s were not recorded). The optimum ink formulation and related values of responses were indicated.

nanocrystals increase the surface area of the optically active *a*-WO_3 matrix, providing a higher number of electrochemically reactive sites. The overall device performance expressed by CE is closely related to the optical modulation and reveals similar behavior as a function of TiO_2/WO_X solid content.

The contour plot on a trilinear coordinate scale was used to present predictions of experimental results obtained via the multiple regression fitting. This graphical methodology provides an easy way to demonstrate the efficacy of the enhanced performance of printed EC films. Ternary plots were generated as a function of TiO_2/WO_X nanocrystalline content while the concentrations of other components (PTA, OAD) were kept constant (Figure 6). The third axis stood for pure alcoholic aqueous solvent in order to quantify the amount of nanocrystals dispersed in the ink and afterward transferred to the printed films. The effect on EC film properties of the type and content of metal oxide nanoparticles in the precursor sol formulated under various peroxopolytungstic acid (PTA) and oxalic acid (OAD) proportions have been comprehensively described elsewhere.[16]

Empirical Model Validation. The model optimality was evaluated on the basis of a summary of the fit (the least-squares regression) and of analysis of variance (ANOVA) parameters, presented in Table 2. The polynomial response modeling (quadratic) offered by the screening design appeared to be sufficient for the optical density (ΔOD) and coloration efficiency (CE) due to its ability to supply high coefficient of determination (R^2-adj) values of 0.87 and 0.98, respectively, indicating a good correspondence between the model prediction (fitting) and the experiments, while simultaneously minimizing the overall number of coefficients. The ANOVA significance probabilities (Prob > F) of 0.0235 and 0.0006, respectively, support the accuracy of the model. In case of coloration time (τ_{col}) and bleaching time (τ_{bl}), the regression coefficients were 0.51 and 0.72, while significance probabilities were 0.2228 and 0.0893, respectively, indicating that the models for those responses are only slightly better than the overall response mean, yielding a small number of significant regression factors. The size of random noise (residual variance), as measured by Normalized Root Mean Square (NRMSE), is reflecting the same prediction abilities for τ_{col}, τ_{bl}, ΔOD, and CE, giving values of 21%, 14%, 10.3%, and 4.5%, respectively. As no nonlinear response was detected for τ_{col} and τ_{bl} (residual by predicted plot with a random pattern—not shown here), a more complex design type is not required, and the lack of fit comes from difficulties associated with accurate measurements of those responses (see section 6 in the Supporting Information for more details).

Briefly, the proposed experimental design methodology was found to offer a sufficiently accurate mathematical modeling with a complete coverage of experimental trials (R^2 values of 0.91, 0.95, 0.98, and 1 for τ_{col}, τ_{bl}, ΔOD, and CE, respectively), while the total number of designed experiments has been reduced from 162 in the full factorial (L = 3) and 72 in the extreme vertices (D = 2) approach, down to only 30 runs.

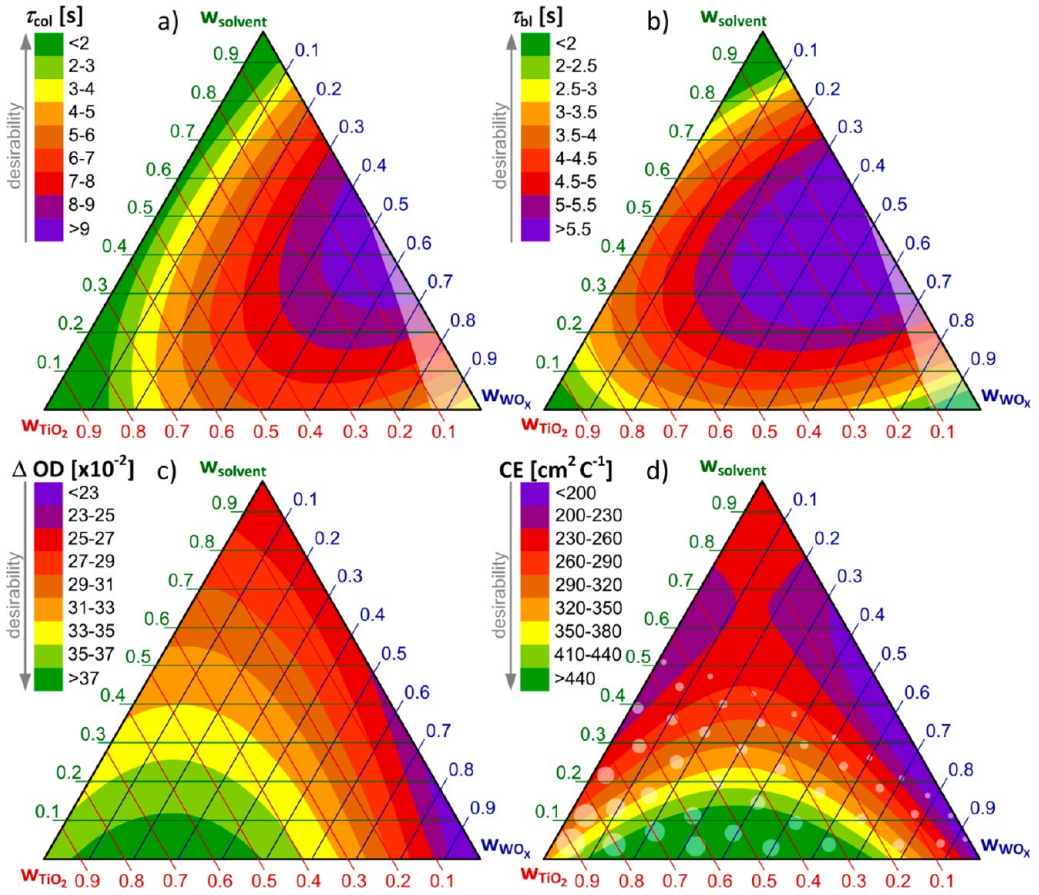

Figure 6. Empirical response contour plots presenting variation in (a) coloration time (τ_{col}), (b) bleaching time (τ_{bl}), (c) optical density (ΔOD), and (d) coloration efficiency (CE) as the weight fractions of TiO_2 and WO_X dispersions are varied (w_{PTA} = 0.01, w_{OAD} = 0.01, X = 3{yellow}, values selected via ink optimization). The triangle faded region indicates unreliable measurements due to the low optical modulation (see section 6 in the Supporting Information for more details), while the region of rounded faded marks indicates concentrations for which discontinuous patterns were obtained (detailed discussion on the influence of film discontinuity on data reliability is presented elswere[16]).

Table 2. Model Validation Parameters

	summary of fit				analysis of variance		
response	R^2	R^2-adj	RMSE[a]	NRMSE[b]	mean	F ratio	Prob > F
τ_{col} (s)	0.91	0.51	2.52 (s)	21.0 (%)	6.25 (s)	2.27	0.2228
τ_{bl} (s)	0.95	0.72	1.40 (s)	14.0 (%)	4.96 (s)	4.13	0.0893
ΔOD (x10^{-2})	0.98	0.87	8.38 (× 10^{-2})	10.3 (%)	27.08 (× 10^{-2})	8.87	0.0235
CE (cm^2 C^{-1})	1	0.98	21.27 (cm^2 C^{-1})	4.5 (%)	169.63 (cm^2 C^{-1})	57.70	0.0006

[a]Root mean square error. [b]Normalized root mean square error: NRMSE = 100·RMSE/($Y_k^{max} - Y_k^{min}$) (%).

Analysis of Significance. The initial tests of significance of all effects (factors and interactions) have been performed graphically using leverage plots.[17] However, due to the complexity of this representation, the leverage graphs are not presented here, but their qualitative results were included in Table 3 (see section 8 in the Supporting Information for more details).

Quantitatively, estimated effects of all factors or their interactions are represented via the absolute value of the t ratio and p value, graphically described in Figure 7. The t ratio shows how strong the evidence is that a selected variable contributes something with additional relevance, while all the other variables in the current model are already taken into account. The p value tests the null hypothesis that each coefficient is statistically zero. A typical value of confidence for rejecting this hypothesis occurs usually for (1 − p value) > 0.95. Thus, a large absolute value of t ratio indicates that the element should be included in the model, while a p value less than 0.05 is regarded as significant.

Analysis results of all effects based on the leverage plots method and Student's t-test statistics for τ_{col}, τ_{bl}, ΔOD, and CE responses lead to the conclusions shown in Table 3. Elements marked by (+) indicate those coefficients that were determined to be significant, meaning that the factor (or factor interactions) had a major effect on a particular response value, quantifying their importance.

As the emphasis of DOE was screening, the *importance* column indicates the most significant effects (starting from value 1) sorted by the absolute value of the t ratio, which lists the test statistics for the hypothesis that each parameter is zero. Each t-ratio value expresses a ratio of particular parameter

dx.doi.org/10.1021/co400011q | ACS Comb. Sci. 2014, 16, 5−16

Table 3. Results of the Factorial Analysis Obtained via the Leverage Plots Method and Student's *t*-Test Statistics

	response model							
	τ_{col}		τ_{bl}		ΔOD		CE	
effect	result[a]	importance	result[a]	importance	result[a]	importance	result[a]	importance
$w_{solvent}$	−		−		+	6	+	3
w_{PTA}	−[b]		+[b]	6	+[b]	2	+[b]	7
w_{OAD}	−[b]		−[b]		−[b]		−[b]	
w_{TiO_2}	−		+	2	+	1	+	1
w_{WO_X}	+	1	+	1	+	5	+	4
$w_{solvent}\cdot w_{PTA}$	−		+	5	+	3	+	10
$w_{solvent}\cdot w_{OAD}$	−		−		−		−	
$w_{solvent}\cdot w_{TiO_2}$	−		−		−		+	6
$w_{solvent}\cdot w_{WO_X}$	+	2	+	3	−		+	16
$w_{solvent}\cdot X$	−		−		−		+	5
$w_{solvent}\cdot w_{TiO_2}$	−		−		−		+	14
$w_{PTA}\cdot w_{TiO_2}$	−		+	7	+	5	+	12
$w_{solvent}\cdot w_{WO_X}$	−		+	4	+	4	+	13
$w_{PTA}\cdot X$	−		−		−		+	9
$w_{OAD}\cdot w_{WO_X}$	−		−		−		−	
$w_{OAD}\cdot w_{WO_X}$	−		−		−		−	
$w_{OAD}\cdot X$	−		−		−		+	8
$w_{TiO_2}\cdot w_{WO_X}$	−		−		−		+	2
$w_{TiO_2}\cdot X$	−		−		−		+	15
$w_{WO_X}\cdot X$	−		−		−		+	11

[a]− Not significant. + Significant. [b]Colinearity.

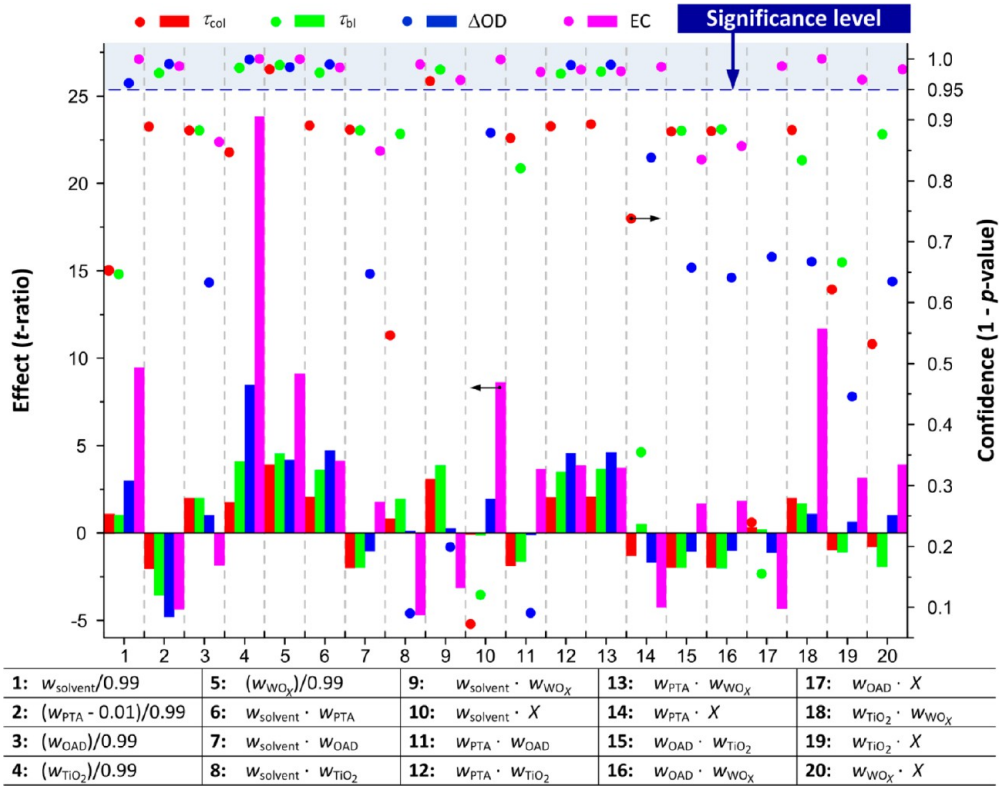

Figure 7. Effect plot for all factors and interactions under consideration in screening design analysis for τ_{col}, τ_{bl}, ΔOD, and CE.

estimate to its standard error and has a Student's *t*-distribution if the hypothesis is true.

In general, the model predicts that EC performance of printed films is enhanced by dual-phase composition, which means that metal oxide nanocrystal concentration is critical. In detail, the significance analysis leads to the conclusion that the τ_{col} depends mainly on the quantity of WO_X nanocrystals in the EC layer. The τ_{bl} is influenced by the quantity of WO_X and

dx.doi.org/10.1021/co400011q | ACS Comb. Sci. 2014, 16, 5−16

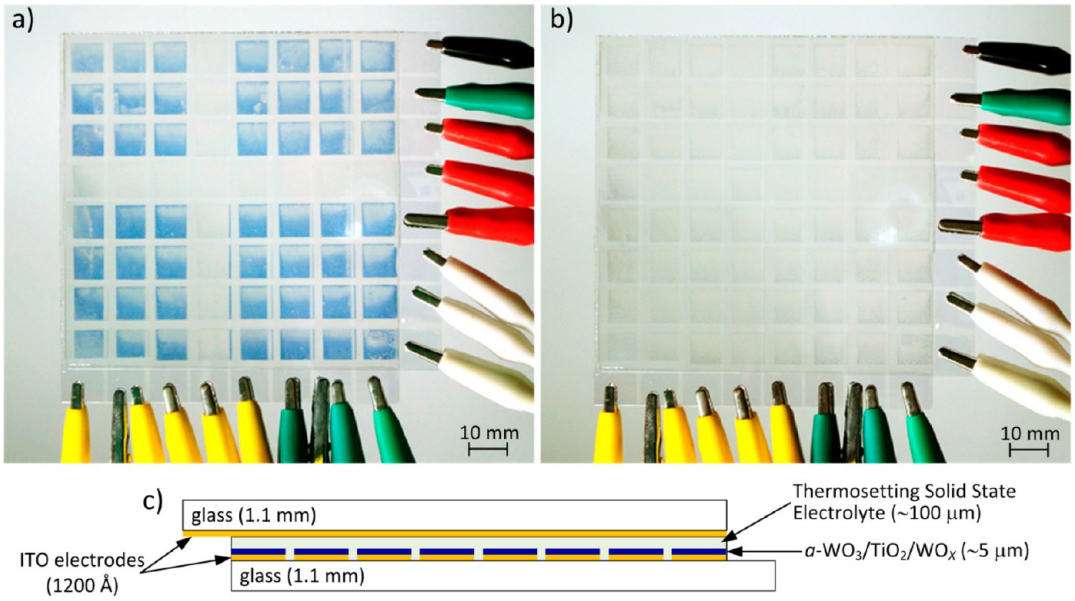

Figure 8. Prototype of inkjet printed all-solid-state EC transparent 8 × 8 passive matrix (100 × 100 mm) on ITO glass substrates in (a) colored and (b) bleached state during operation and its (c) schematic cross section with thickness values of each layer.

TiO_2 nanocrystals and also depends of the WO_3 amorphous content formed from the PTA precursor. The ΔOD, which describes the optical contrast between colored and bleached states, depends mainly on the quantity of TiO_2 nanocrystals and WO_3 amorphous content. The significant factors with regards to their impact on CE, which describes overall device performance, depends to a greater or lesser extent on almost all mixture components and their interactions, but the most significant are TiO_2 and WO_X crystalline nanoparticles. The colinearity indicated by (∗) obtained for main effects derived from PTA and OAD components indicates that those two coefficients have no independent variation to support fitting to any presented response variation, because they are linear functions of other factors. While the role of PTA is evident from coefficients of the first order interactions, the OAD impact on the EC performance is almost negligible. The OAD component may therefore be eliminated from consideration without detriment to the EC effect, simplifying the method by reducing the number of ingredients. However, as will be shown in following sections, that small amount of OAD ($w_{OAD} = 0.01$) was identified as a component in optimal ink formulation.

Ink Optimization. One of the reasons to fit a mathematical model to experimental data is to find combinations of the component proportions in a mixture setting, to reach the maximum possible performance. Response surface maps of experimental regions presented in Figures 5 and 6 facilitate the decision-making process when determining the most appropriate ink formulation for desired individual EC responses. However, a numerical multiresponse optimization offered by software enables one to find the specific point that maximizes the global desirability, and thus, optimal overall EC performance.[18] In such simultaneous optimization, the desirability values (d_k) of n responses (Y_k) are combined to create an overall desirability (D) as described by eq 9. Such definition ensures that if any single desirability is equal to zero (undesirable), the overall desirability is 0 as well.

$$D = (\Pi_{k=1}^{n} d_k^{I_k})^{1/\sum_{k=1}^{n} I_k} = (\Pi_{k=1}^{n} f_k(Y_k)^{W_k \cdot I_k})^{1/\sum_{k=1}^{n} I_k} \quad (9)$$

Thus, W_k is the weight, I_k is the significance and the one-sided function $f_k(Y_k)$ depends on the response's optimization goal (minimize or maximize) according to eq 10 showing maximization of Y_k response (minimization is equivalent to maximization of $-Y_k$).

$$f_k(Y_k) = \begin{cases} 0, & Y_k \le Y_k^{min} \\ \left(\dfrac{Y_k - Y_k^{min}}{Y_k^{max} - Y_k^{min}}\right), & Y_k^{min} < Y_k < Y_k^{max} \\ 1, & Y_k \ge Y_k^{max} \end{cases} \quad (10)$$

The applied desirability function $f_k(Y_k)$ is a transformation of each estimated response variable to the desirability value on a 0 to 1 scale, where 0 represents a completely undesirable response and 1 represents the most desirable response.

In order to determine the best performing EC ink formulation, the optimization goal was to minimize values of coloration and bleaching times and maximize values of the optical density and coloration efficiency. Weights and importance values were set as equal ($W_k = I_k = 1$), while desired response limits (Y_k^{min}, Y_k^{m}) were defined according to the experimental results (indicated in Table 1), which simplifies the overall desirability to the geometric mean of individual desirability values expressed by eq 11.

$$D = (\Pi_{k=1}^{n} d_k)^{1/n} = (\Pi_{k=1}^{n} f_k(Y_k))^{1/n} \quad (11)$$

The resulting optimum ink formulation is described by the following factor values (wt %): $w_{solvent} = 0$, $w_{PTA} = 0.01$, $w_{OAD} = 0.01$, $w_{TiO_2} = 0.76$, $w_{WO_X} = 0.22$, and $X = 3\{yellow\}$, yielding the maximum overall desirability value of 0.89. The examination of results from the desirability profiler gives the performance prediction for an optimized EC device in which $\tau_{col} = 3.3$ s, $\tau_{bl} = 2.8$ s, ΔOD = 0.38, and CE = 480 $cm^2\ C^{-1}$ (see Figure 5d), thereby fulfilling all of the optimization requirements.

Prototype. An 8 × 8 EC passive matrix consisting of two 100 mm by 90 mm glass substrates with 64 pixels, 1 cm^2 each, is shown in Figure 8. When applying a voltage to a selected pair

dx.doi.org/10.1021/co400011q | ACS Comb. Sci. 2014, 16, 5−16

of electrodes, the ions are driven from the electrolyte into a-WO_3/TiO_2/WO_X film, where they are intercalated causing the chromatic effect (Figure 8a). Reversing the voltage returns them to the electrolyte, resulting in the pixels' bleaching (Figure 8b). Although the performance measurements of the prototype were not carried out according to the methodology described in the Experimental Procedures, it is evident that the matrix exhibits high optical contrast, while the switching time is comparable to those of the fastest lab-testing devices developed according to DOE recipes.

EXPERIMENTAL PROCEDURES

Design Generation. A screening design has been performed according to the Design of Experiment methodology using JMP 8.0 statistical software (S.A.S. Institute Inc., Cary, NC, USA). Flexible JMP's Custom Designer has been applied to determine the main factors and interaction effects and to investigate the changes of the responses by varying each factor in order to predict the device performance for all possible ink recipe combinations. The D-optimal design using 30 runs is shown in Table 4 and Figure 4. Please note that the final design for the same input parameters may be different depending on the software used, as different procedures for generating D-optimal designs can be implemented.

Table 4. The List of Experimental Trials (Design Matrix) According to the *Mixture Design with One Non-Mixture Component* Methodology

	factors					
	mixture components					categorical
run number	$w_{solvent}$ (wt)	w_{PTA} (wt)	w_{OAD} (wt)	w_{TiO_2}(wt)	w_{WO_x}(wt)	X
1	0.539	0.010	0	0	0.451	yellow
2	0	0.200	0	0	0.800	blue
3	0	0.113	0.050	0.837	0	blue
4	0	0.200	0	0.800	0	yellow
5	0.800	0.200	0	0	0	yellow
6	0.575	0.010	0	0.415	0	yellow
7	0	0.010	0.050	0	0.940	blue
8	0	0.010	0.050	0.940	0	yellow
9	0	0.010	0	0.498	0.492	blue
10	0.940	0.010	0.050	0	0	yellow
11	0	0.010	0	0	0.990	yellow
12	0	0.200	0.050	0	0.750	blue
13	0	0.010	0	0	0.990	blue
14	0	0.010	0	0.990	0	yellow
15	0	0.200	0	0	0.800	yellow
16	0.465	0.010	0.026	0	0.499	blue
17[a]	0.940	0.010	0.050	0	0	blue
18[a]	0.800	0.200	0	0	0	blue
19	0.866	0.109	0.025	0	0	yellow
20	0.441	0.010	0.026	0.523	0	blue
21	0	0.081	0.024	0.445	0.451	yellow
22[a]	0	0.010	0	0.990	0	blue
23	0	0.200	0.023	0.777	0	blue
24	0	0.200	0.050	0.750	0	yellow
25	0.990	0.010	0	0	0	blue
26[a]	0	0.010	0.050	0.940	0	blue
27	0.351	0.200	0.050	0	0.399	yellow
28	0	0.010	0.050	0	0.940	yellow
29	0.401	0.108	0	0.491	0	blue
30	0.750	0.200	0.050	0	0	blue

[a]Duplicates.

Ink Formulation. Peroxopolytungstic acid (PTA) was synthesized on the basis of the procedure reported by Kudo et al.[19,20] The tungsten metal monocrystalline powder (Aldrich, 0.6−1 μm, 99.9%) was carefully added to a 50 mL mixture (50:50) of distilled water (Millipore) and hydrogen peroxide (Sigma-Aldrich, 30% by weight). The cooling was employed, and the solution was kept slowly stirring for 24 h in a refrigerator to prevent thermal changes due to the strong exothermic nature of the dissolution. The excess of tungsten powder was then removed by filtration (Roth, 0.45 μm syringe filter), leading to a transparent solution. In order to remove the excess of hydrogen peroxide, the solution was dried at 65 °C and washed several times with the distilled water. After drying, a water-soluble orange crystal powder (PTA)[21] was obtained. It should be noted that the PTA synthesized in the present study and used as a sol−gel precursor of the amorphous phase may differ from the ones presented by other authors in terms of composition. The PTA expressed by empirical formula $WO_3 \cdot xH_2O_2 \cdot yH_2O$ was found to be crystalline or amorphous depending on x.[20] The H_2O_2 content depends of the applied evaporation procedure (hot plate, N_2 bubbling or rotary evaporation) in precursor synthesis[21,22] and storage conditions; therefore obtaining reproducible products in different laboratories is difficult. Although an analytical determination of x and y was not performed in the present study, it was observed that the solid obtained from PTA has an amorphous structure and is easily soluble in water at RT. As it is known from elsewhere,[20] such properties indicate that the synthesized substance has a structure expressed by formula $WO_3 \cdot (1 > x \geq 0.53)H_2O_2 \cdot (1.5 > y \geq 3)H_2O$. It was therefore expected that the variable amount of cheating peroxo groups $[O_2]^{2-}$ may affect morphological evolution during the film formation and post-treatment, and thus result in different EC performance. As it was crucial to obtain reproducible products for a full set of designed experiments, the synthesis was optimized to ensure its repeatability by implementation of a very detailed protocol. Additionally, in order to unify the input material for an ink formulation, products of many syntheses were mixed and ground together. As the PTA crystals are known for their instability, the final product was stored at low temperature (−18 °C).

Two types of commercially available WO_X nanoparticles were used as a source of crystalline phase, WO_3 referred to as yellow (Aldrich, < 100 nm) and $WO_{2.9}$ referred to as blue (Super Conductor Materials, 99.99%, ceramic oxide target, ∼30 nm). Titania paste (Solaronix, Ti-Nanoxide T/SC, 15−20 nm, 3% by weight) was used as a source of nanocrystalline TiO_2. These nanoparticles were used in a form of aqueous (Millipore) alcohol (Merck, 2-propanol, 99.8%) dispersions in a fixed proportion of 30:70 and a solid content of 0.01% by weight. The oxalic acid dihydrate (Merck) was used as received.

In order to obtain 3 g of gel electrolyte, 0.36 g of PMMA (Fluka), 0.21 g of PEO−PPO (Zeon Chemicals), 0.33 g of $LiClO_4$ (Fluka), and 1.75 g of propylene carbonate (Fluka, 99%) were mixed with 4 mL of tetrahydrofuran (Aldrich, 99.9%) and followed by stirring for about 4 h until a transparent uniform lightly viscous gel was obtained.[23]

Inkjet Printing. An ink was formulated according to the DOE recipe for each lab-testing device. Particular layers (1 cm^2) were printed using a modified Canon PIXMA IP4850 desktop printer (see section 1 in the Supporting Information

for detailed printing system description) in regular intervals of around 1 min while being exposed to a relative humidity of 50%, at 28 °C on ITO PET substrates (Sigma-Aldrich, 1000 Å of ITO, 60 Ω/sq, T > 75% at 550 nm). All films were dried at room temperature for 24 h and annealed in the air at 120 °C (EHRET, TK4067, Germany) for 1 h.

Encapsulation. The lab-testing devices were assembled as a sandwich structure, which includes inkjet printed EC film (working electrode), a gel electrolyte for ion storage, and two transparent conductors (ITO PET foil) separated by a double-sided tape spacer (1 mm thick). The device has been sealed with thermoplastic glue (see section 3 in the Supporting Information for detailed procedure).

Prototype Development. A prototype of transparent EC 8 × 8 passive matrix was produced according to the structure presented in Figure 8c in the following steps: (i) wet etching of ITO conductive tracks substrate (0.1 M HCl at 60 °C as etching solution; 10 mm wide scotch tape was used to mask the ITO) on two 100 mm by 90 mm glass substrates (Xin Yan Technology, 1200 Å of ITO, 10 Ω/sq, T > 85% at 550 nm), (ii) inkjet printing of optimized a-$WO_3/TiO_2/WO_X$ ink formulation, (iii) film annealing for 1 h in the air at 120 °C (EHRET, TK4067, Germany), (iv) drop-casting of thermosetting composite solid state electrolyte (manuscript describing this material system is under preparation), (v) sandwiching with a counter electrode, and (vi) *in situ* electrolyte curing under ambient conditions.

Characterization Techniques. The structural analysis of EC printed films was supported by SEM measurements (Auriga SEM-FIB, Zeiss). Optical measurements were performed using a spectrometer setup consisting of an HR4000 High-Resolution Spectrometer (Ocean Optics), Halogen Light Source HL-2000-FHSA (Mikropack), High Current Source Measure Unit (KEITHLEY 238), and QP600-2-SR/BX optical fibers (type, SR; core diameter, 600 μm; connector, QSMA; jacketing, BX). The spectral response was measured in a wide range of wavelengths (400−900 nm) for the films colored and bleached after a constant time period (1 min) at operating voltage values of 4 and −4 V, respectively (see section 5 in the Supporting Information for a detailed system description). The electrochemical measurements (Gamry Reference 600 Potentiostat, Gamry Instruments) were performed on assembled devices in a two-electrode configuration in which *working* and *working sense* are connected to a working electrode and *reference* and *counter* are connected to a second (ITO) electrode (see section 4 in the Supporting Information for detailed system description).

CONCLUSIONS

This work demonstrated that a combination of IPT as a novel deposition technique and the DOE methodology provides an effective means to explore and predict the behavior of high performance EC devices. Using the D-optimal mixture design with one no-mixture component could reduce the total number of experimental trials from 162 in the full factorial (L = 3) and 72 in the extreme vertices (D = 2) approach down to only 30 runs, while still maintaining a high accuracy of analysis. Very high determination coefficients of the empirical models have proven the method's ability to predict the optimal ink formulation. The inkjet printed EC films show outstanding performance when comparing with the state-of-the-art counterparts derived from analogous precursors via other deposition techniques. Coloration and bleaching time of optimized films reached 3.3 and 2.8 s, respectively (state-of-the-art: coloration time of 20−35 s for dip-coated,[24,25] 30−53 s for spin-coated,[25,26] and 94 s for electrodeposited[27,28] films; bleaching time typically of 5−20 s[25−28]). Optical modulation of 0.38 is comparable to other films derived from PTA.[26,29,30] Superior overall performance of the optimized films is reflected in coloration efficiency reaching 480 cm^2 C^{-1} (state-of-the-art: 40−60 cm^2 C^{-1} for dip-coated,[25] 40−55 cm^2 C^{-1} for spin-coated,[25,29] and 60 cm^2 C^{-1} for electrodeposited[27,28] films). The identification of the critical process factors via the screening experiment was essential for method optimization itself and resulted in a reduced number of system components, greatly simplifying the technological process.

ASSOCIATED CONTENT

Supporting Information

Several diagrams, pictures, and plots are provided for more detailed description of the methodology, arguments, and conclusions presented. They provide information about the inkjet printing system, ink formulation details, EC device encapsulation, electrochemical measurements setup, optical measurements setup, definitions of parameters (responses), design diagnostic, and initial tests of significance (leverage plots). Moreover, a short movie is attached, so as to facilitate the understanding of the method presented. This material is available free of charge via the Internet at http://pubs.acs.org.

AUTHOR INFORMATION

Corresponding Authors

*Tel.: (+351) 21 294 8562. Fax: (+351) 21 294 8558. E-mail: p.wojcik@campus.fct.unl.pt.

*Tel.: (+351) 21 294 8562. Fax: (+351) 21 294 8558. E-mail: emf@fct.unl.pt.

Notes

The authors declare no competing financial interest.

ACKNOWLEDGMENTS

This work was funded by the Portuguese Science Foundation (FCT-MCTES) through project Electra, PTDC/CTM/099124/2008 and the PhD grant SFRH/BD/45224/2008 given to P. J. Wojcik. Moreover, this work was also supported by E. Fortunato's ERC 2008 Advanced Grant (INVISIBLE contract number 228144), "APPLE" FP7-NMP-2010-SME/262782-2 and "SMART-EC" FP7-ICT-2009.3.9/258203.

REFERENCES

(1) Glasnov, T. N.; Tye, H.; Kappe, C. O. *Tetrahedron* **2008**, *64*, 2035−2041.

(2) Altekar, M.; Homon, C.; Kashem, M.; Mason, S.; Nelson, R.; Patnaude, L.; Yingling, J.; Taylor, P. *JALA (1998-2010)* **2006**, *11*, 33−41.

(3) Lu, W.-B.; Kao, W.-C.; Shi, J.-J.; Chang, J.-S. *J. Hazard. Mater.* **2008**, *153*, 372−81.

(4) Vanatta, L.; Coleman, D.; Woodruff, A. *J. Chromatogr. A* **2003**, *997*, 269−278.

(5) Tye, H. *Drug Discovery Today* **2004**, *9*, 485−91.

(6) Qazi, S.; Samuel, N. K. P.; Venkatachalam, T. K.; Uckun, F. M. *Int. J. Pharm.* **2003**, *252*, 27−39.

(7) Rosario, A. V.; Pereira, E. C. *Sol. Energy Mater. Sol. Cells* **2002**, *71*, 41−50.

(8) Calvert, P. *Chem. Mater.* **2001**, *13*, 3299−3305.

(9) Derby, B. *Annu. Rev. Mater. Res.* **2010**, *40*, 395−414.

(10) Cornell, J. *Experiments with Mixtures: Design, Models, and the Analysis of Mixture Data*, 3rd ed.; John Wiley & Sons, Inc.: New York, 2002.

(11) McLeane, R. A.; Anderson, V. L. *Technometrics* **1966**, *8*, 447−454.
(12) Bacon, D. W.; Lott, R. In *Quality improvement through statistical methods*; Springer: New York, 1998; p 237.
(13) *JMP 8 Design of Experiments Guide*, Second Edition; SAS Institute Inc: Cary, NC, 2009.
(14) Eriksson, L. *Design of Experiments: Principles and Applications*; Umetrics Academy: Umeå, Sweden, 2008.
(15) Smith, W. F. *Experimental Design for Formulation*; Society for Industrial and Applied Mathematics: Philadelphia, PA, 2005.
(16) Wojcik, P. J.; Cruz, A. S.; Santos, L.; Pereira, L.; Martins, R.; Fortunato, E. *J. Mater. Chem.* **2012**, *22*, 13268.
(17) Sall, J. *Am. Stat.* **1990**, *44*, 308−315.
(18) Derringer, G.; Suich, R. *J. Qual. Technol.* **1980**, *12*, 214−219.
(19) Yamanaka, K.; Oakamoto, H.; Kidou, H.; Kudo, T. *Jpn. J. Appl. Phys.* **1986**, *25*, 1420−1426.
(20) Okamoto, H.; Ishikawa, A.; Kudo, T. *Bull. Chem. Soc. Jpn.* **1989**, *62*, 2723−2724.
(21) Pecquenard, B.; Castro-Garcia, S.; Livage, J.; Zavalij, P. Y.; Whittingham, M. S.; Thouvenot, R. *Chem. Mater.* **1998**, *10*, 1882−1888.
(22) Kim, C.-Y.; Lee, M.; Huh, S.-H.; Kim, E.-K. *J. Sol-Gel Sci. Technol.* **2009**, *53*, 176−183.
(23) Barbosa, P. C.; Rodrigues, L. C.; Silva, M. M.; Smith, M. J.; Valente, P. B.; Gonçalves, A.; Fortunato, E. *Polym. Adv. Technol.* **2011**, *22*, 1753−1759.
(24) Taylor, D. J.; Cronin, J. P.; Allard, L. F.; Birniem, D. P. *Chem. Mater.* **1996**, *8*, 1396−1401.
(25) Deepa, M.; Saxena, T.; Singh, D.; Sood, K.; Agnihotry, S. *Electrochim. Acta* **2006**, *51*, 1974−1989.
(26) Işık, D.; Ak, M.; Durucan, C. *Thin Solid Films* **2009**, *518*, 104−111.
(27) Deepa, M.; Srivastava, A.; Saxena, T.; Agnihotry, S. *Appl. Surf. Sci.* **2005**, *252*, 1568−1580.
(28) Deepa, M.; Kar, M.; Agnihotry, S. A. *Thin Solid Films* **2004**, *468*, 32−42.
(29) Choy, J.-H.; Kim, Y.-I.; Yoon, J.-B.; Choy, S.-H. *J. Mater. Chem.* **2001**, *11*, 1506−1513.
(30) Wu, W.-T.; Liao, W.-P.; Chen, J.-S.; Wu, J.-J. *ChemPhysChem* **2010**, *11*, 3306−12.